Eur. Phys. J. A **14**, 377–392 (2002)
DOI 10.1140/epja/i2002-10008-x

THE EUROPEAN PHYSICAL JOURNAL A

Approximation of photonuclear interaction cross-sections

M.V. Kossov[a]

ITEP, Moscow, Russia and CERN, 1211 Geneva, Switzerland

Received: 22 February 2002 / Revised version: 17 April 2002
Communicated by M. Garçon

Abstract. Photonuclear interaction cross-sections from the GEANT4 database are approximated for all nuclei and all energies (from the hadron production threshold to about 40 TeV). The approximation methods in the giant-dipole resonance region, nucleon resonance region, and high-energy region are improved with respect to existing approximations. As an application of the approximation for photonuclear cross-sections, an improved method of calculating electronuclear cross-sections is developed. The interaction cross-section of virtual photons with nuclei at high Q^2 are approximated and a simple algorithm for describing the electronuclear reactions, including high-Q^2 scattering, is proposed.

PACS. 25.20.-x Photonuclear reactions – 25.30.Rw Electroproduction reactions – 24.30.-v Resonance reactions – 21.60.Ka Monte Carlo models

1 Introduction

Reproduction of the photonuclear and electronuclear reactions is very important for the simulation of electromagnetic showers, as they are the only reactions converting electromagnetic energy of electrons, positrons, and photons to hadronic energy of mesons, nuclear fragments, and soft neutrons. For the simulation of photonuclear and electronuclear reactions it is necessary to devise a general method of approximation of the known experimental cross-sections over a very wide energy range. The simulation toolkit GEANT4 [1] includes simulation of nuclear fragmentation in the photonuclear and electronuclear reactions on the basis of the CHIPS model [2–4].

A database of the measured $\gamma A \to hadrons$ interaction cross-sections is created in the GEANT4 environment. For applications it is approximated and extrapolated. The approximation of the energy dependence of photonuclear cross-sections is subdivided into three main regions: the giant-dipole resonance (GDR) region, the nucleon resonance (N^*) region, and the high-energy region. In each of these regions there are independent methods of approximation. Most of these methods do not take into account the tails of contributions from the neighboring regions. In this paper the general method of approximation for all nuclei and for all energies above the hadron production threshold is developed. Hence the emphasis is less on the physics concepts than on the empirical fitting procedure. Nevertheless, the general fit can give insight into a few fundamental effects, such as collective modes of excitation of nuclear giant resonance, "melting" of high nucleon resonances in nuclear matter, and the non-saturated unitarity in the high-energy extrapolation of the photonuclear cross-sections.

The $\sigma_{\gamma p}$ cross-section, discussed in sect. 2, is fundamental for all photonuclear cross-sections. The energy dependence of the $\sigma_{\gamma p}$ cross-sections is the only source of information for the extrapolation of photonuclear cross-sections to energies above 1 TeV. This is considered in sect. 3. In the N^* region, $\sigma_{\gamma p}$ is a starting point for the analysis of the modification of the nucleon resonances in the nuclear matter. In this region the $\ln(E)$ scale is used for the approximation of the resonance shape, instead of the Breit-Wigner formula which uses a linear E scale. The $\ln(E)$ scale was chosen because, on the one hand, it is convenient for the integrals necessary for the calculation of electronuclear interaction cross-sections, and, on the other hand, because the extrapolation to 40 TeV (as shown in sect. 3) is described by the $\ln(E)$ function. This approximation procedure in the N^* region is discussed in sect. 4.

In all three regions the known approximation procedures are improved. In the GDR region the method of multinucleon excitations is used to fit not only the GDR maxima of different shapes, but also the cross-sections in the so-called quasi-deuteron region (between the traditional GDR region and the Δ-resonance region). The approximation procedure for the interaction cross-sections below the pion production threshold is discussed in sect. 5.

In sect. 6 the main emphasis is on the definition of the photonuclear cross-sections for the virtual photons at high Q^2. Three different approaches are compared: equivalent photons approximation (EPA), transverse photon flux (TPF), and deep-inelastic scattering (DIS) structure

[a] e-mail: Mikhail.Kossov@cern.ch

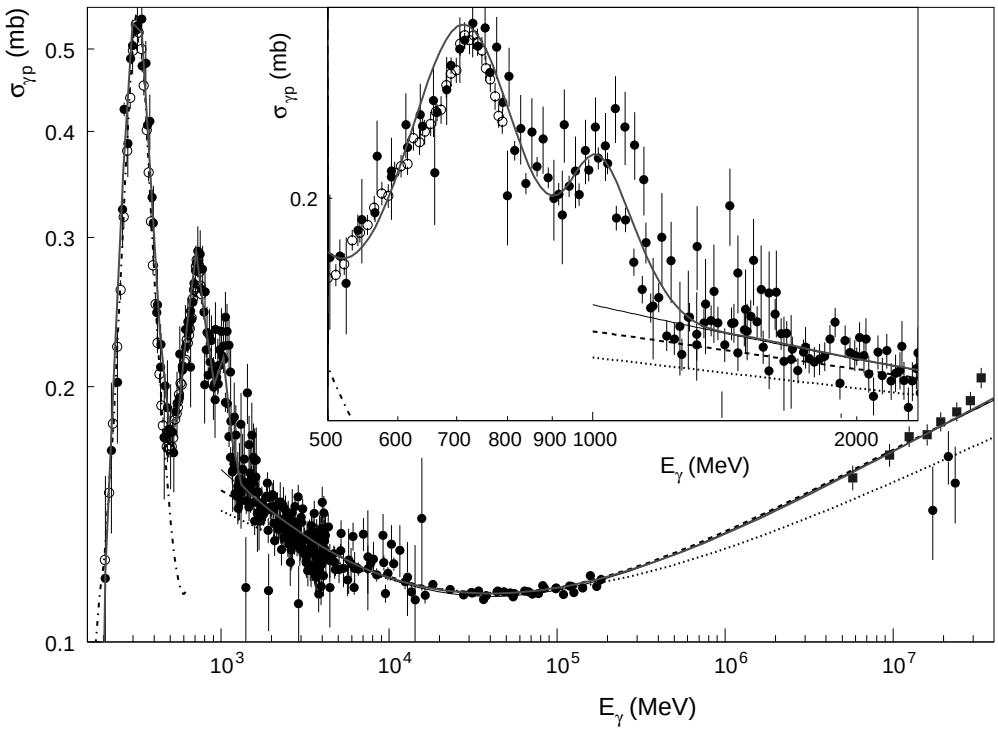

Fig. 1. The $\sigma_{\gamma p}$ cross-section. Filled circles correspond to the PDG collection [5], empty circles correspond to the Mainz data [6], and squares correspond to the HERA data [7]. The dotted line is the Froissart bound $\ln^2(s)$ approximation, the dashed line is the non-saturated unitarity $\ln(s)$ approximation, the thin solid line is the $\ln(E)$ approximation, and the thick solid line is the resulting GEANT4 approximation (at high energies it coincides with the thin solid and the dashed lines). The dash-dotted line at low energies shows the approximation based on partial-wave analysis [8].

functions. All the three approaches have different normalization of the photonuclear cross-sections at high Q^2. Clarification of this normalization difference is very important for comparison of experimental measurements, and for development of the simulation algorithm. The simple approximation for the virtual photon interactions with nuclei is used for simulation of the electronuclear reactions with high Q^2. This method needs further improvement. In the GDR region an additional Q^2-dependent form factor must be used and at high energies the nuclear shadowing factor must be changed. Unfortunately the appropriate measurements are not available, so at present this improvement cannot be made.

2 Interaction of photons with protons

For the analysis of the $\sigma_{\gamma p}$ cross-sections, the PDG data set [5] is used together with the recent data from Mainz [6] and HERA [7]. The data are shown in fig. 1. In all figures of this paper the interaction cross-sections are in units of mb. The thick solid line shows the final GEANT4 approximation of the data set. This figure can be used to illustrate the $\ln(E)$ resonance shape and the method of threshold functions, which are used in the GEANT4 approximation.

The $\ln(E)$ resonance formula is similar to the Breit-Wigner formula

$$r(E) = \frac{v}{1 + \frac{(\ln(E)-u)^2}{w}}, \tag{1}$$

where E is the photon energy in the laboratory system measured in MeV, v is the amplitude of the resonance, w is the relative squared half-width of the resonance, and u is the position of the resonance on the $\ln(E)$ scale. The flow factor E^{-2} is not used in this approximation so the positions of resonances are artificially shifted to lower energies. This formula is used for the Δ-resonance and for the effective resonance (the sum of a few close resonances at $E \approx 750\,\mathrm{MeV}$). The effective resonances above 900 MeV for the γp and γd interactions have relatively small amplitudes. They are formally approximated by the g_4- and g_8-functions defined in sect. 5.

The method of threshold functions is used to restrict contributions of different interaction mechanisms. For the $\sigma_{\gamma p}$ cross-sections the tail of the Δ-resonance contribution must not cover the region below the π^0 production threshold. To cut this tail, a threshold function of the form

$$f(E) = (1 + e^{(\tau - \ln(E))\cdot\xi})^{-1}, \tag{2}$$

is used, where τ is the threshold position and ξ characterizes the slope of the threshold. The threshold functions are used for the N^*-resonance contributions, so for complex nuclei the tails of the nucleon resonances (defined by

the widths of resonances) do not contribute to the low-energy region. For photonuclear cross-sections the pion production threshold may be A-dependent, as pions can be produced by interactions with nuclear clusters and the Δ-resonance can decay through the $\Delta N \to NN$ channel. Thus, the modification of the threshold position $\tau(A)$ in nuclear matter is possible, as are modifications of the amplitude ($v(A)$), position ($u(A)$), and width ($w(A)$) of the resonances. Another threshold function is used for the artificial subdivision between the explicit resonance contributions and the continuous Regge-pole contribution, which has the $s^{-\eta}$ form and is usually limited by some minimum energy.

The threshold function plays a fundamental role in the approximation in the GDR region. This method of approximation of the photonuclear cross-sections is discussed in detail in sect. 5. The threshold function smoothly reduces the contributions of the processes below the threshold. To make the low-energy cross-section below the hadron production threshold go to zero, the simple additional threshold condition (a θ-function, which is 0 below the threshold and 1 above the threshold) is used for the kinematically defined hadron production threshold. For protons the hadron production threshold is defined by the π^0 mass, while for nuclei it is defined by the minimum separation energy.

The only γp interaction mechanism below the π^0 production threshold is Compton scattering. For a point-like charged particle with spin $\frac{1}{2}$ and zero anomalous momentum this was calculated by Klein and Nishina [9]. The anomalous magnetic momentum contribution for the point-like particle was calculated by Powell [10]. The structure of the nucleon was taken into account by Petrun'kin [11] in the form of the electric and magnetic polarizabilities $\bar{\alpha}$ and $\bar{\beta}$. Usually the Compton scattering on nuclei is not taken into account in the simulation as the cross-section of the γp Compton scattering is about five orders of magnitude smaller than that for photon-electron Compton scattering. But Compton scattering by electrons is concentrated at small angles, while Compton scattering by protons in the 30–130 MeV energy range is almost isotropic and energy independent ($\frac{\mathrm{d}\sigma}{\mathrm{d}\Omega} \approx 15\,\mathrm{nb/sr}$) [12]. Therefore Compton scattering by protons can be important for the simulation of electromagnetic showers in hydrogen-rich media when large-angle scattering of photons is important.

3 Photonuclear interactions at high energies

Approximation of $\sigma_{\gamma p}$ and σ_{hp} cross-sections at high energies was made in [13] for the full set of the PDG data. Two approximation formulas for the Froissart bound [14] (saturated unitarity) case

$$S(E) = P \cdot (A + B \cdot \ln^2(s)) + R \cdot s^{-\eta} \tag{3}$$

and for the non-saturated unitarity [15] case

$$\bar{S}(E) = P \cdot (A + B \cdot \ln(s)) + R \cdot s^{-\eta} \tag{4}$$

were tested. The η, A, and B parameters obtained in [13] are common for the approximations of the γp and the hp interactions. For the different incident particles only the P and R parameters are different. It was found that the non-saturated unitarity formula (eq. (4)) is a better approximation at low energies. In our paper this formula is improved by the substitution $s = 2M_pE$ (M_p is the proton mass). For this case the approximation formula is

$$h(E) = a \cdot (\ln(E) - c) + b \cdot E^{-d}. \tag{5}$$

The parameters a, b, c, and d are calculated from parameters A, B, P, R, and η, so this approximation is in accordance with the global fit of the hadron-proton cross-section made in [13]. The dotted line in fig. 1 shows the Froissart bound approximation (eq. (3)), the dashed line corresponds to the non-saturated unitarity formula (eq. (4)), and the thin solid line corresponds to eq. (5). At high energies the last two obviously coincide with, and approximate the new HERA measurements much better than the Froissart bound formula. The thick solid line shows the resulting GEANT4 approximation of the $\sigma_{\gamma p}$ cross-sections:

$$\sigma_{\gamma p} = f_r \cdot (r_\Delta + r_H) + g_4 + g_8 + f_p \cdot h_p^{(p)}, \tag{6}$$

where

$$f_r = (1 + e^{25\cdot(5.24-z)})^{-1}, \tag{7}$$

$$r_\Delta = \frac{0.55}{1 + \frac{(z-u_\Delta(1))^2}{w_\Delta(1)}}, \tag{8}$$

$$u_\Delta(A) = 5.82 - \frac{0.07}{1 + 0.003 \cdot A^2}, \tag{9}$$

$$w_\Delta(A) = 0.056 + \ln(A) \cdot (0.03 - 0.001 \cdot \ln(A)), \tag{10}$$

$$r_H = \frac{0.223}{1 + \frac{(z-6.57)^2}{w_H(1)}}, \tag{11}$$

$$w_H(A) = 0.045 + 0.04 \cdot (\ln(A))^{\frac{3}{2}}, \tag{12}$$

$$g_4 = \frac{e^{4\cdot(6.27-z)}}{1 + e^{12\cdot(7.25-z)}}, \tag{13}$$

$$g_8 = \frac{e^{8\cdot(6.66-z)}}{1 + e^{24\cdot(6.9-z)}}, \tag{14}$$

$$f_p = (1 + e^{4\cdot(7-z)})^{-1}, \tag{15}$$

$$h_p^{(p)} = 0.0375 \cdot (z - 16.5) + 1.07 \cdot e^{-0.11\cdot z}, \tag{16}$$

and $z = \ln(E)$. There is no GDR maximum for protons, so the two fake GDR terms g_4 and g_8 are used to improve the approximation in the high N^*-resonance region ($E > 900\,\mathrm{MeV}$). The g-functions are defined in sect. 5. They were used for the approximation of the high resonance contributions to the γp and γd cross-sections to avoid additional terms in the general A-dependent approximation formula. It should be noted that the three A-dependent functions $u_\Delta(A)$, $w_\Delta(A)$, $w_H(A)$ and the A-independent f_p-function are defined starting from the hydrogen nucleus.

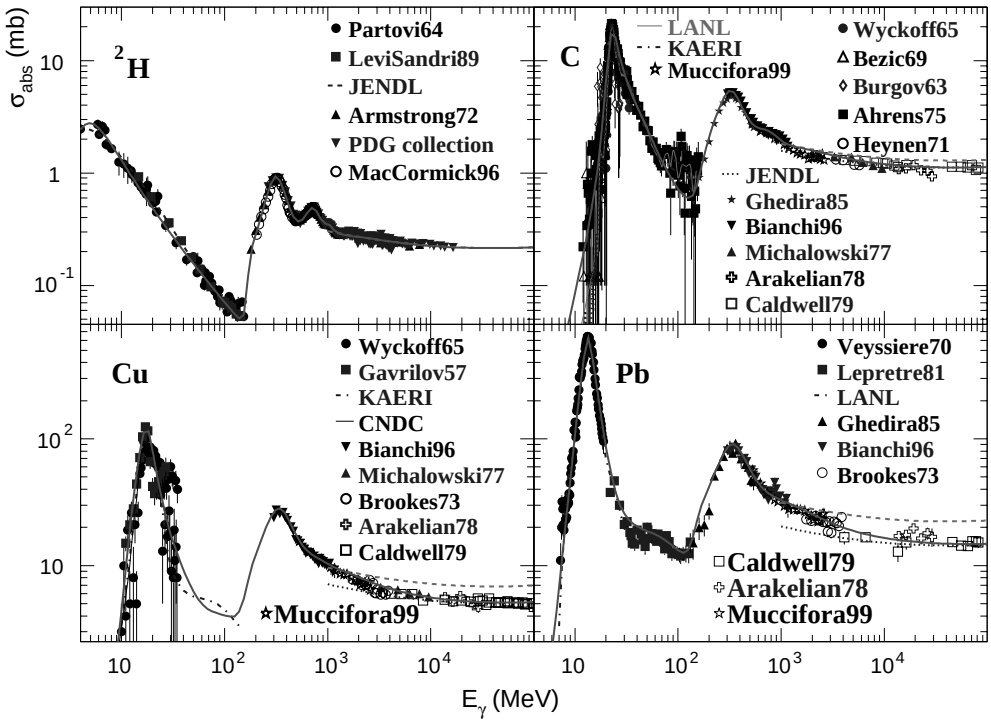

Fig. 2. Photonuclear interaction cross-sections. References to the [16–55,6,56–69] data set are named after the first author and by the year of publication, the known GDR approximations are from the internationally available computerized library EXFOR (LANL-USA, BOFODM-Russia, KAERI-S. Korea, JENDL-Japan, CNDC-China). The thick solid line is the GEANT4 approximation. The dashed line is the h_p part of the ^{2}H cross-section (without the f_p threshold factor) multiplied by $\frac{A}{2}$. The dotted line is the same function, but normalized by the GEANT4 shadowing factor $s_p(A)$ (eq. (26)).

In the Δ-resonance region the GEANT4 approximation is compared with the approximation resulting from the partial-wave analysis [8] (the curve is taken from [12]), which underestimates the cross-section above 480 MeV. The two Δ-resonance approximations are different only at $E < 200$ MeV. Measurements of the $\sigma_{\gamma p}$ cross-sections in this energy region are not available.

The photonuclear cross-sections are only measured up to $E = 100$ GeV, so additional assumptions about the A-dependence of the photonuclear cross-sections must be used to extrapolate the existing data set to infinite energies. The general picture of photonuclear cross-sections is shown in fig. 2 where the GEANT4 approximation is shown by the thick solid line. If the atomic weight is not indicated explicitly in the figures the measurements are done with the natural mixture of isotopes. Unlike the γp data, the γd data have the well-known photodisintegration part, which is a precursor of the GDR maxima for complex nuclei. So the γd data are approximated by an equation similar to eq. (6) with two additional terms g_1 and g_2, which correspond to the GDR terms for the complex nuclei:

$$\sigma_{\gamma d} = f_r(r_\Delta + r_H) + g_1 + g_2 + g_4 + g_8 + s_p(2) f_p h_p(2), \quad (17)$$

where

$$f_r = (1 + e^{25\cdot(\tau_r(2)-z)})^{-1}, \quad (18)$$

$$\tau_r(A) = 5.13 - 0.00075 \cdot A, \quad (19)$$

$$r_\Delta = \frac{0.88}{1 + \frac{(z-u_\Delta(2))^2}{w_\Delta(2)}}, \quad (20)$$

$$r_H = \frac{0.348}{1 + \frac{(z-6.575)^2}{w_H(2)}}, \quad (21)$$

$$g_1 = \frac{e^{1\cdot(1.86-z)}}{1 + e^{3\cdot(1.2-z)}}, \quad (22)$$

$$g_2 = \frac{e^{2\cdot(2.11-z)}}{1 + e^{6\cdot(1.5-z)}}, \quad (23)$$

$$g_4 = \frac{e^{4\cdot(6.2-z)}}{1 + e^{12\cdot(7.1-z)}}, \quad (24)$$

$$g_8 = \frac{e^{8\cdot(6.62-z)}}{1 + e^{24\cdot(6.91-z)}}, \quad (25)$$

$$s_p(A) = A \cdot (1 - 0.072 \cdot \ln(A)), \quad (26)$$

$$h_p(A) = 0.0375 \cdot (z - 16.5) + s_h(A) \cdot e^{-0.11\cdot z}, \quad (27)$$

$$s_h(A) = 1.0663 - 0.0023 \cdot \ln(A). \quad (28)$$

The g_4- and g_8- GDR functions are still formally used to improve approximation in the high-resonance region. The $\tau_r(A)$ threshold function and the $s_p(A)$ shadowing function are universal for all complex nuclei starting from deuterium. The $s_p(A)$ function is the only function which normalizes the high-energy photonuclear cross-sections taking into account the nuclear shadowing effect [70].

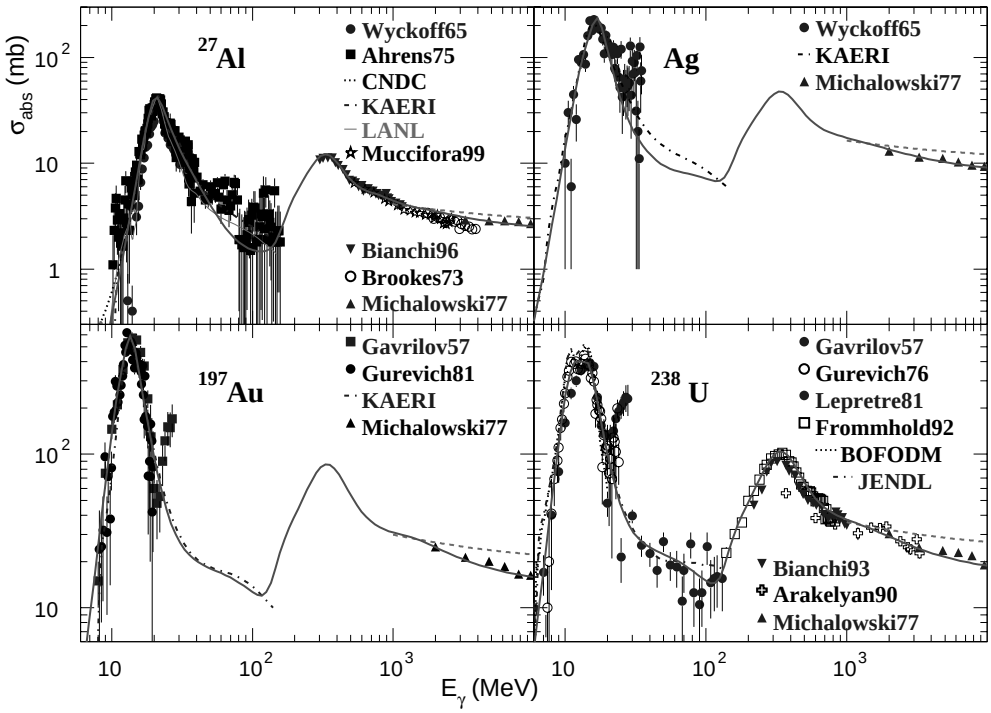

Fig. 3. Photonuclear interaction cross-sections for Al, Ag, Au, and U nuclei. References are the same as in fig. 2.

The high-energy approximation for γd reactions is reproduced in two forms for C, Cu, and Pb nuclei. The first form is the γd cross-section multiplied by the $\frac{A}{2}$ factor (dashed lines), another form is normalized by the $s_p(A)$ factor (dotted line). Because of the nuclear shadowing, the high-energy contribution to the photonuclear cross-sections drops with increasing A, and the upper tails of the resonance terms make a relatively larger contribution for heavier nuclei in the 1–10 GeV region. That is why the GEANT4 approximation curve differs from the dotted lines in this region. To compensate for these increasing resonance contributions, and to keep the GEANT4 approximation close to the dotted line up to 40 TeV, it is necessary to use an additional function $s_h(A)$ for shadowing of the Regge-pole contribution. The $s_h(A)$ function is general for all complex nuclei starting from deuterium.

4 Photonuclear interactions in the resonance region

The resonance part for nuclei heavier than deuterium is approximated by two contributions: by the Δ-resonance contribution and by the effective resonance contribution, which sums the contributions of resonances above 500 MeV.

The photonuclear interaction cross-sections in the resonance region are shown in fig. 3 and fig. 4. The A-dependence of the resonance contribution can be approximated by eq. (17) with the following functions:

$$f_r = (1 + e^{11\cdot(\tau_r(A)-z)})^{-1}, \tag{29}$$

$$r_\Delta = \frac{0.39 \cdot A}{1 + \frac{(z-u_\Delta(A))^2}{w_\Delta(A)}}, \tag{30}$$

$$r_H = \frac{\frac{0.16\cdot A}{\sqrt{\ln(A)}}}{1 + \frac{(z-u_H(A))^2}{w_H(A)}}, \tag{31}$$

$$u_H(A) = 6.496 + 0.042 \cdot \ln(A). \tag{32}$$

For complex nuclei the threshold of the resonance contribution is shifted to lower energies. The most probable reason for this seems to be the additional $\Delta N \to NN$ decay channel for the Δ-resonance in nuclear matter. The threshold $\tau_r(A)$ was found to decrease linearly with increasing A (eq. (19)). For uranium it is shifted by about 25 MeV.

The position of the Δ-resonance maximum (eq. (9)) is found to be shifted to higher energies for heavy nuclei. For γp reactions the Δ maximum is at $M = 1212$ MeV and for the photon-uranium reactions it is at $M = 1229$ MeV. For light nuclei this shift is negligible and for heavy nuclei it is almost constant.

Broadening of the Δ-resonance contribution is characterized by the $w_\Delta(A)$ function (eq. (10)). No shadowing is found in the resonance region. This conclusion confirms the rough estimate made in [71]. The logarithmic A-dependence of the position of the effective resonance (eq. (32)) and the A-dependence of its width (eq. (12)) are partially determined by the necessary compensation for the artificial threshold of the high-energy Regge-pole contribution, and cannot characterize real shift and broadening for the group of resonances.

Comparison of the $\sigma_{\gamma p}$ and the σ_{hp} cross-sections with the photonuclear cross-sections for heavy nuclei shows

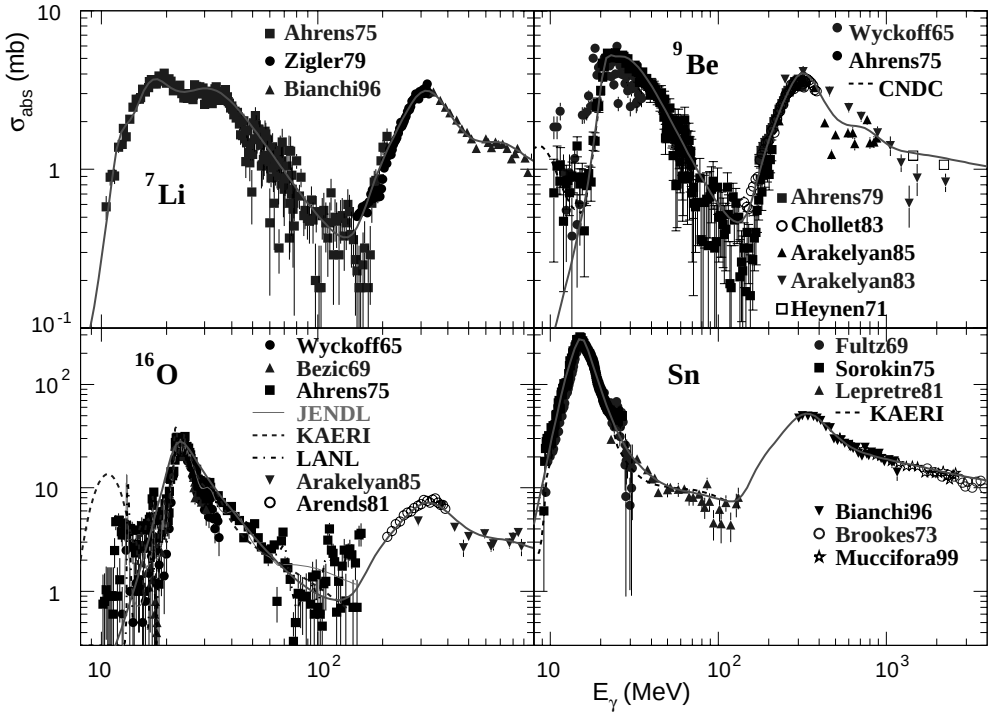

Fig. 4. Photonuclear interaction cross-sections for ^{7}Li, Be, O, and Sn nuclei. References are the same as in fig. 2.

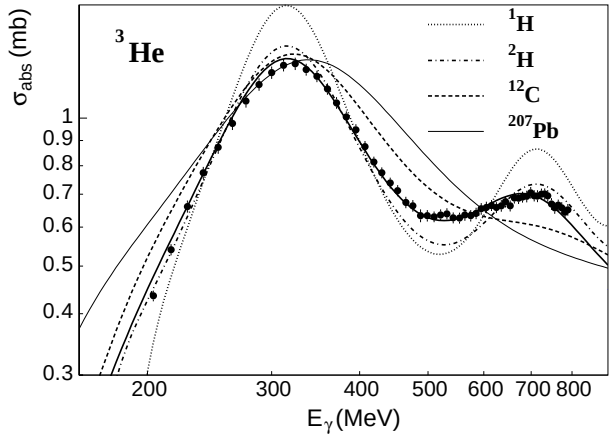

Fig. 5. Photonuclear interaction cross-sections for ^{3}He nuclei. The points are from [6], and the thick solid line is the GEANT4 approximation for ^{3}He. For comparison the approximation curves (normalized by the factor $\frac{3}{A}$) are shown for ^{1}H (dotted line), ^{2}H (dash-dotted line), C (dashed line), and Pb (thin solid line).

that the effective resonance at 750 MeV is significantly reduced ("melted") for heavy nuclei. The high resonances, which are described by the g_4- and g_8-functions for the hydrogen and deuterium targets, are not seen at all in the interactions of photons with complex nuclei. To illustrate the effect of "melting" of resonances, the data for ^{3}He are shown in fig. 5 together with the normalized GEANT4 approximation functions for ^{1}H, ^{2}H, C, and Pb nuclei. The GEANT4 approximation reflects the "melting" effect, but to simulate the subsequent nuclear fragmentation it is necessary to have a model describing this effect. It would be very interesting to measure the photonuclear cross-section on ^{3}He, ^{4}He, ^{6}Li, and ^{7}Li nuclei up to 1.5 GeV to discover the "melting" mechanism for the resonances excited at photon energies higher than 900 MeV.

5 Photonuclear interactions in the GDR region

Photonuclear interaction cross-sections in the GDR region are approximated as a sum of four functions which are defined as

$$g_i = \frac{e^{i\cdot(\rho_i - z)}}{1 + e^{3i\cdot(\tau_i - z)}}, \tag{33}$$

where $i = 1, 2, 4, 8$. These functions are powers of $\frac{1}{E}$ reduced by the threshold function at low energies. One can think of each rescattering of the photon by the nucleon as adding one power of $\frac{1}{E}$ to the cross-section. Because of the binding energy, or Pauli blocking for heavy nuclei, the amplitude of each rescattering can be equally suppressed, such that the same power (but multiplied by the factor 3) appears in the resulting threshold functions. The minimal set of the powers of the g-functions was determined by the widths of the measured GDR maxima. This is an empirical choice of g-functions. The four selected functions allow us to describe a wide variety of shapes of the GDR maxima. The shapes are complicated for light nuclei, while for heavy nuclei they are close to the traditional Lorentzian function $L(E) \propto (\Gamma_r^2 + \frac{(E^2 - E_r^2)^2}{E^2})^{-1}$.

The lightest nuclei are compared with heavy nuclei in fig. 6. The relatively big γ-^{6}Li cross-section in compari-

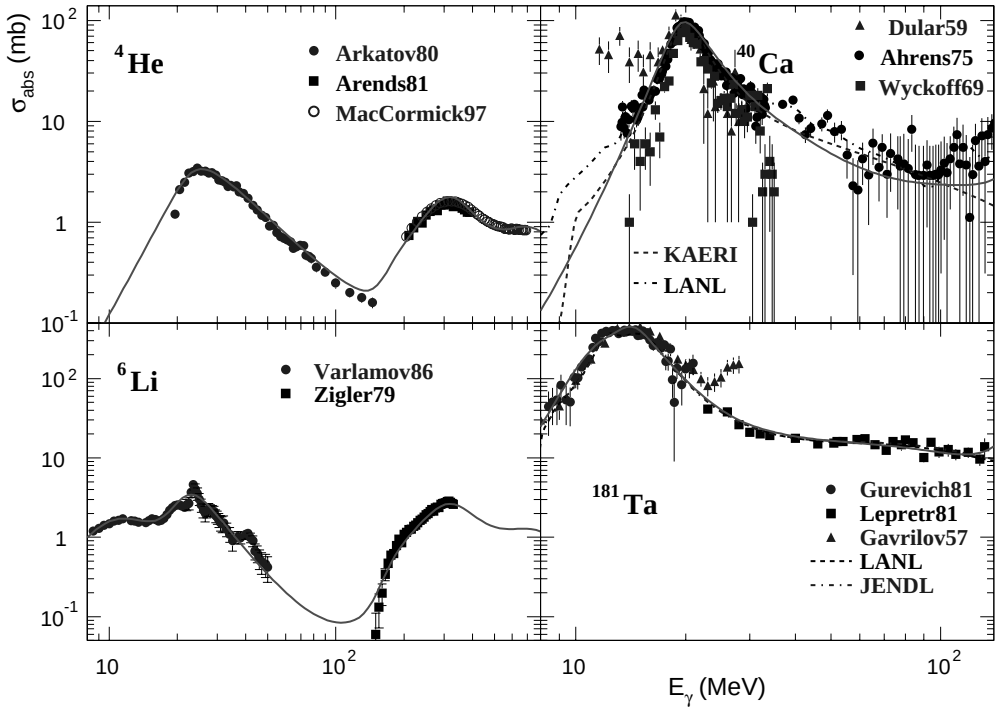

Fig. 6. Photonuclear interaction cross-sections for ^{4}He, ^{6}Li, Ca, and Ta nuclei. References are the same as in fig. 2.

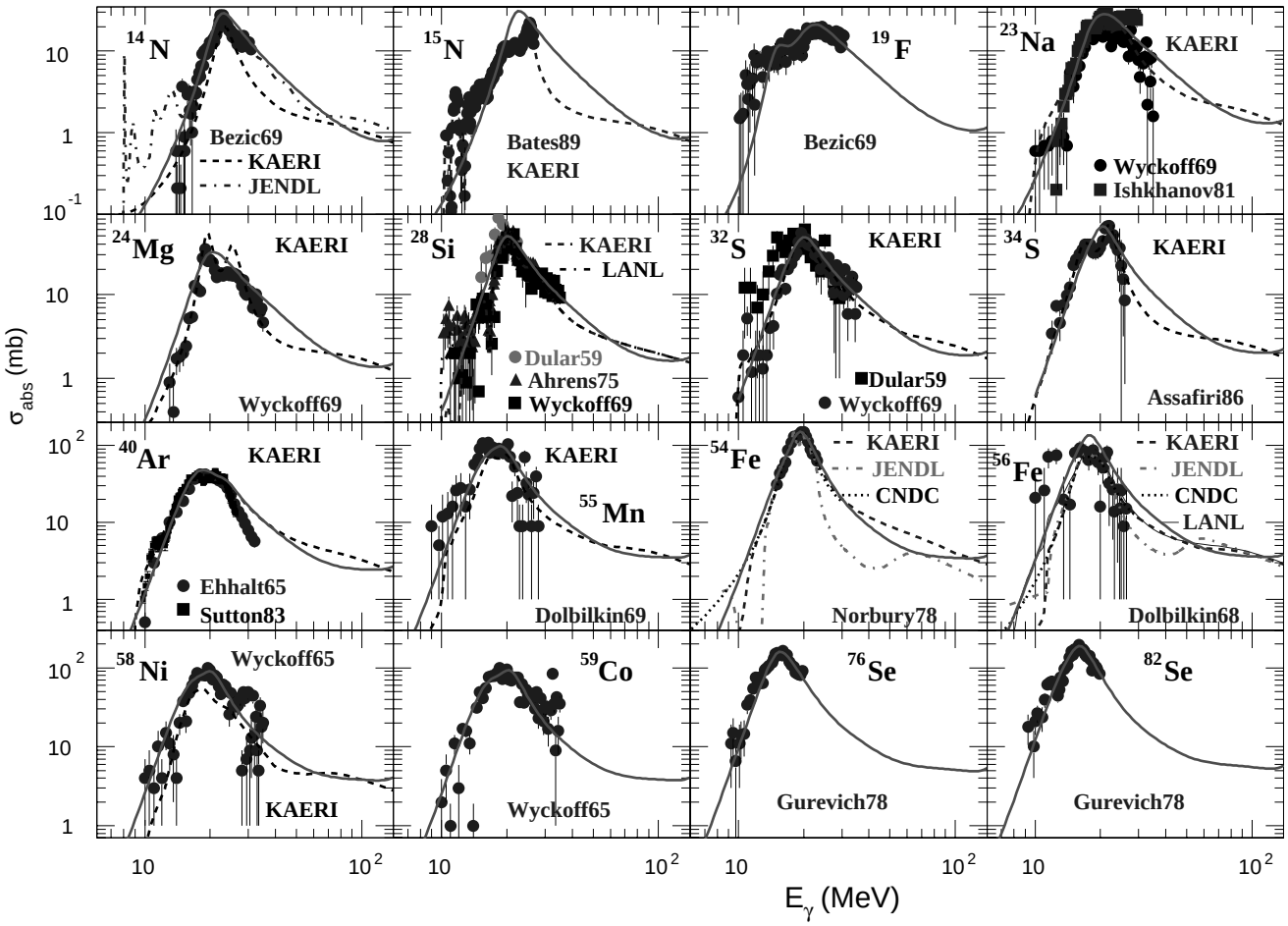

Fig. 7. Photonuclear interaction cross-sections in the GDR region for the medium nuclei. References are the same as in fig. 2.

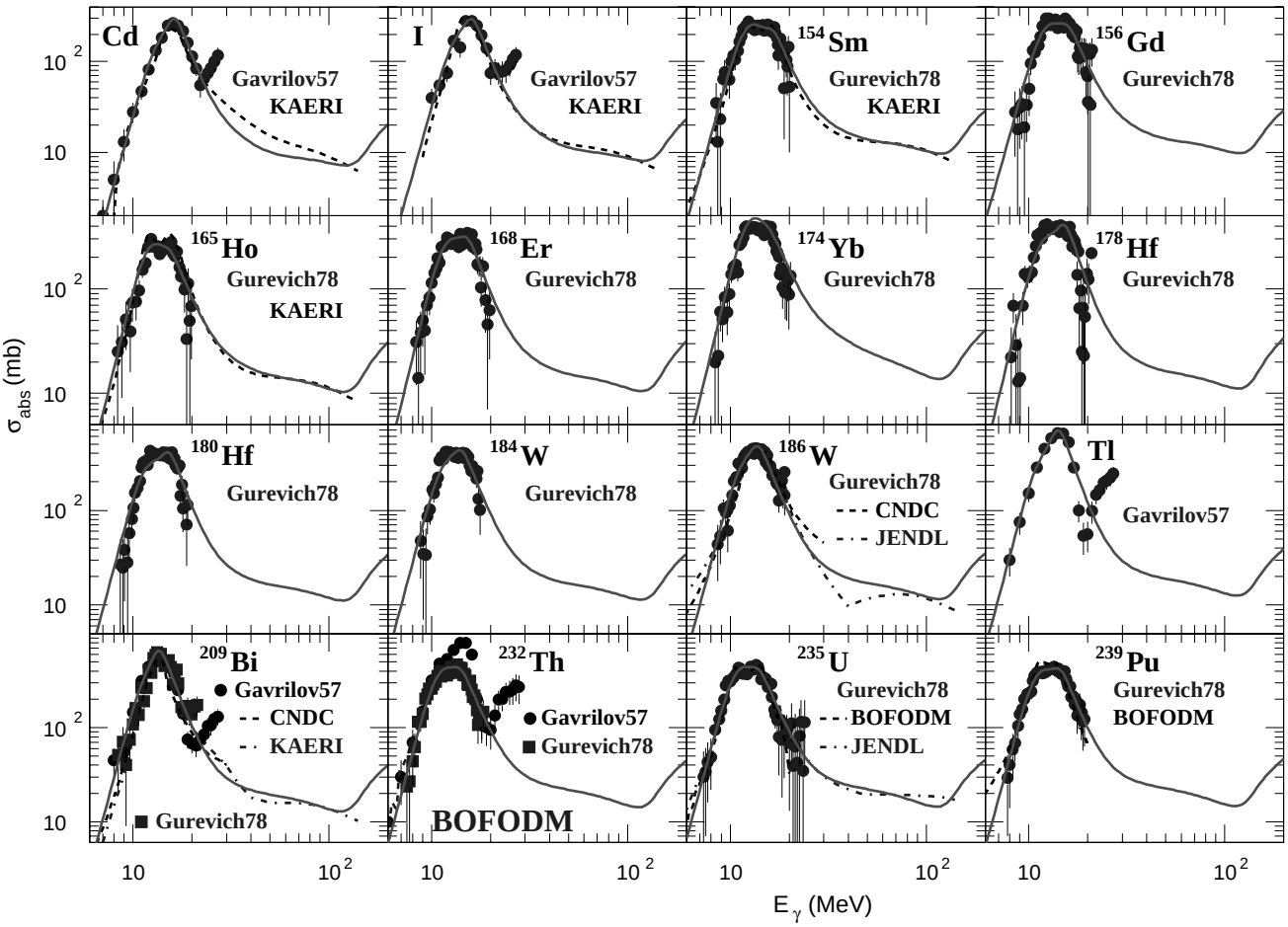

Fig. 8. Photonuclear interaction cross-sections in the GDR region for heavy nuclei. References are the same as in fig. 2.

son to γ-^{4}He and γ-^{7}Li cross-sections at 10 MeV (fig. 4) is noteworthy. Another interesting effect can be found at 100 MeV (the so-called quasi-deuteron region), where the prominent GDR maximum has already dropped and the energy is still not sufficient to excite the Δ-resonance. Two measurements [16,54] cover this region for light and heavy nuclei, respectively. Additional information about this region can be obtained by the analysis of the ^{4}He data (the GDR maximum drops steeply), and of the ^{6}Li data (the pion production threshold drops to a very low level). So it appears that, for the lightest nuclei, the cross-section in this region is relatively small.

The rest of the data for medium nuclei are shown in fig. 7. It is clear from the figure that the experimental measurements and the existing extrapolations have very specific systematic errors. That is why it is not only useful to compare different measurements for the same nucleus, but also to develop the A-dependent approximation which can help to suppress the systematic errors when comparing the measurements for different nuclei. The g_1-, g_2-, and g_4-functions for the lightest nuclei, and the g_8-function for all the nuclei, have individual values for each nucleus. This helps to describe such differences as that between the ^{40}Ca data (fig. 6, where the maximum reaches 100 mb) and the

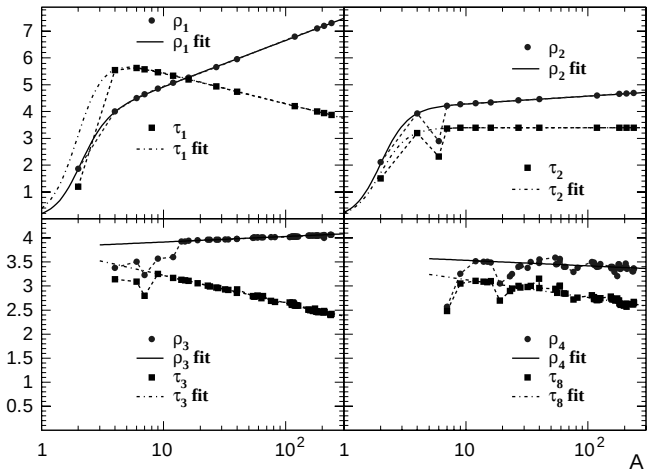

Fig. 9. A-dependence of the ρ and τ parameters of the g-functions used for approximation of the photonuclear interaction cross-sections in the GDR region. The dashed lines connect the subsequent points and the solid and the dash-dotted lines correspond to eqs. (34)-(41).

^{40}Ar data (fig. 7, where the maximum reaches only 50 mb) or the anomalous threshold effect for the ^{19}F data.

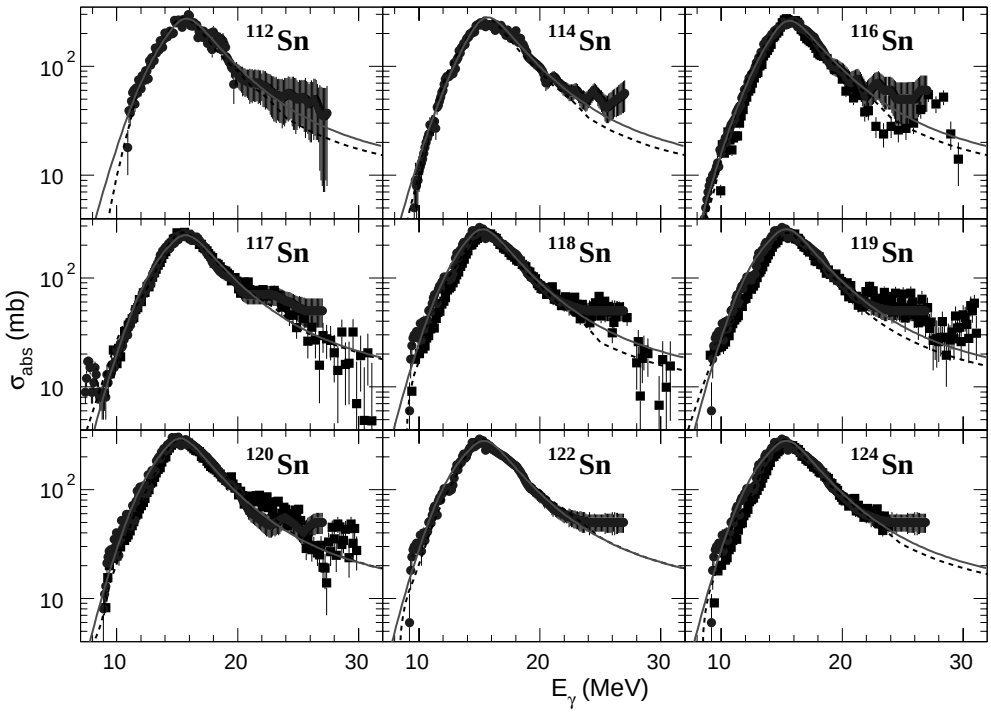

Fig. 10. Photonuclear interaction cross-sections in the GDR region for Sn isotopes. Circles are from [63] and [64], squares are from [44], the dashed line is the KAERI approximation, and the solid line is the GEANT4 approximation.

The rest of the data for heavy nuclei is shown in fig. 8. The well-known effect of broadening of the GDR maximum for the elliptical nuclei is reproduced by the GEANT4 approximation. This effect is prominent for the heaviest nuclei and for the nuclei from Sm to W.

The A-dependence of parameters of the g_i-functions is shown in fig. 9. For the approximation of the A-dependence of the g_1 and g_2 contributions only those nuclei which have measurements in the quasi-deuteron region (around 100 MeV) are selected. Only the g_1- and g_2-functions are used to parametrize the GDR maximum for deuterium, so the "quasi-deuteron" name qualitatively reflects the nature of the contribution of these two functions. With only two exceptions (discussed in a moment) the A-dependence of these functions is smoothly approximated by functions:

$$\rho_1 = \frac{3.2 + 0.75 \cdot \ln(A)}{1 + (\frac{2}{A})^4}, \tag{34}$$

$$\tau_1 = \frac{6.6 - 0.5 \cdot \ln(A)}{1 + (\frac{2}{A})^4}, \tag{35}$$

$$\rho_2 = \frac{4.0 + 0.125 \cdot \ln(A)}{1 + (\frac{2}{A})^4}, \tag{36}$$

$$\tau_2 = \frac{3.4}{1 + (\frac{2}{A})^4}. \tag{37}$$

Both the thresholds and the weights of these contributions appear to grow as a power of A (as ρ_i and τ_i are in exponent), but are sharply reduced by the "A-threshold" function $(1 + (\frac{2}{A})^4)^{-1}$. The "$A$-threshold" function is defined by the fourth power of A, and so must be taken into account only for the lightest nuclei with $A < 4$. The two exceptions are the reduced weight of the g_1-function for the ^{2}H nuclei and the reduced weight and threshold of the g_2-function for the ^{6}Li nuclei. The first exception can be understood as a consequence of the weak binding of nucleons in the ^{2}H nuclei. To understand the second exception for the ^{6}Li nuclei it is necessary to take into account that when the first nucleon is knocked out the residual ^{5}He or ^{5}Li nucleus is unstable, so the threshold for the second separation is negative.

The g_4 and g_8 terms do not contribute to the cross-sections for the nuclei with $A < 4$, so the corresponding approximation functions are much simpler:

$$\rho_4 = 3.8 + 0.05 \cdot \ln(A), \tag{38}$$

$$\tau_4 = 3.8 - .25 \cdot \ln(A), \tag{39}$$

$$\rho_8 = 3.65 - 0.05 \cdot \ln(A), \tag{40}$$

$$\tau_8 = 3.5 + 0.16 \cdot \ln(A). \tag{41}$$

From fig. 9 it is clear that when A is comparable with the value of the index of the g-function, it is necessary to use individual approximation of the $\rho_i(A)$ and $\tau_i(A)$ functions. The coefficients of the g_8-functions are less regular than those of other g-functions because the g_8 contribution is narrow and very sensitive to the systematic errors of measurements using the variable bin Penfold-Leiss method [72], which usually demands subsequent smoothing. This smoothing was not always done as a number of

older theoretical papers predicted narrow maxima in the GDR region.

Two minima are noteworthy: the minimum in the A-dependence of the g_4-function for ^{7}Li and the minimum in the A-dependence of the g_8-function for ^{19}F. The nature of these dips is not clear.

To estimate the isotopic dependence of the GDR maximum the isotopes of Sn are compared to the GEANT4 approximation in fig. 10. The approximation is good for all nine isotopes, so there is no special isotopic dependence for heavy nuclei. Nevertheless the big difference between the ^{40}Ar and the ^{40}Ca data proves that, for the medium and light nuclei, such a dependence can occur.

The expansion over g_i-functions can be applied to other reactions where the GDR is excited. An example of such process is a $A(e,e'p)$ reaction, when the residual $(A-1)$ nucleus can be in the GDR final state. The latest Jefferson Laboratory data [73] for the $^{16}\mathrm{O}(e,e'p)$ reaction ($|\theta_{pq}| = 8^\circ$) is shown in fig. 11(a). Unfortunately the differential cross-sections are presented in the $\frac{p_e E_e p_p E_p \mathrm{d}\sigma^6}{\mathrm{d}^3 p_e \mathrm{d}^3 p_p}$ form instead of the simple relativistically invariant $\frac{E_e E_p \mathrm{d}\sigma^6}{\mathrm{d}^3 p_e \mathrm{d}^3 p_p}$ form, but even the published points show that the g_i contributions with large i are shifted to lower energies when compared with the γA reactions. The reason for this may be the "one-hole" nature of the effect. The "hole" is left when a proton is knocked out. The contributions of g-functions with small i correspond to the s-shell holes, and the contributions of g-functions with large i correspond to the p-shell holes, having more nucleons in their vicinity. The "hole" in the p-shell (or higher shells) can be made with a much smaller energy transfer. For γA reactions, when the momentum transferred to the excited nucleus is as large as the transferred energy, this explanation no longer applies.

Another reaction is the nuclear GDR excitation in heavy-ion collisions. The data of the LAND collaboration [74] for the ^{136}Xe projectile excitation by a ^{207}Pb target are shown in fig. 11(b) together with the g_i fit. In [74] the same data were analysed in terms of the isoscalar giant-monopole resonance, isovector giant-dipole resonance, and isoscalar quadruple resonance, which can be compared with the g_1-, g_2-, and g_4-functions. To describe this data the authors consider the fourth, the so-called "Double GDR" term, which corresponds to the g_8 term of our approximation. In reactions of this kind the contributions of the g_i-functions with large i seem to be shifted to higher energies (this is natural because of the large value of the charge product zZ for such contributions). For reactions of this type the transferred momentum is very large, so at high transferred energy the large transferred momentum is more likely to be absorbed by bigger nuclear clusters than by only one or two nucleons. This may explain the shift of the g_i contributions. From the point of view of the transferred momentum, the γA reactions lie between the "knock out" reactions and the heavy-ion excitation reactions. The common nature of all three effects helps to highlight the mechanism of GDR excitation.

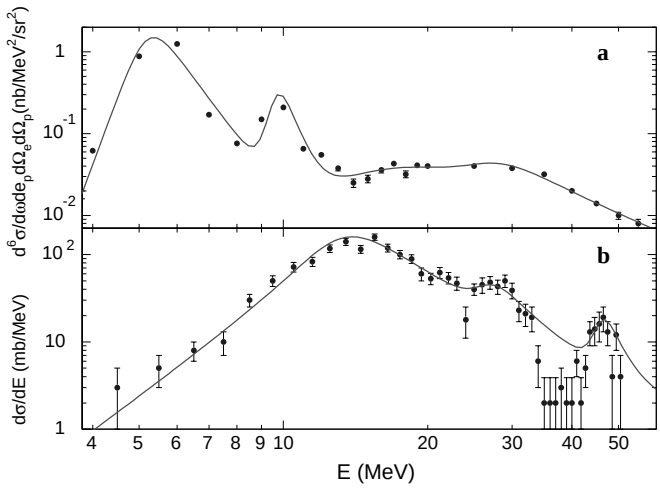

Fig. 11. Photonuclear interaction cross-sections in the GDR approximation formula to (a) $^{16}\mathrm{O}(e,e'p)$ reactions [73], (b) $\mathrm{Xe} + \mathrm{Pb} \to \mathrm{Xe}^* + \mathrm{Pb}$ reaction [74].

6 Application of photonuclear cross-sections to electronuclear reactions

Electronuclear reactions are so closely connected with photonuclear reactions that sometimes they are called "photonuclear" because the one-photon exchange mechanism dominates in electronuclear reactions. In this sense electrons can be substituted by the flux of equivalent photons. This is not completely true, as at high energies the Vector Dominance Model (VDM) or diffractive mechanisms are possible, but these types of reactions are beyond the scope of this paper.

6.1 Common notation for different approaches to the electronuclear reactions

The equivalent photon approximation (EPA) was proposed by E. Fermi [75] and developed by C. Weizsacker and E. Williams [76] and by L. Landau and E. Lifshitz [77]. The covariant form of the EPA method was developed in [78] and [79]. When using this method it is necessary to take into account that real photons are always transversely polarized while virtual photons may be longitudinally polarized. In general the differential cross-section of the electronuclear interaction can be written as

$$\frac{\mathrm{d}^2\sigma}{\mathrm{d}y\mathrm{d}Q^2} = \frac{\alpha}{\pi Q^2}(S_{\mathrm{TL}} \cdot (\sigma_{\mathrm{T}} + \sigma_{\mathrm{L}}) - S_{\mathrm{L}} \cdot \sigma_{\mathrm{L}}). \qquad (42)$$

In earlier papers the authors of the EPA method emphasized that the main photon flux is concentrated at small Q^2, and tried to limit the method by the region where transverse equivalent photons dominate (small y and small Q^2). In later calculations the cross-section of the interaction of longitudinal photons (σ_{L}) was postulated to be negligible and with this assumption the method was generalized for any y and Q^2. It was a good assumption for

the application of the equivalent photon method to e^+e^- reactions where the $\gamma\gamma$ interactions at high energies were calculated [80,81]. The electronuclear process was considered in these papers as a "connected" process with the following expressions for the $S_{\rm TL}$ and $S_{\rm L}$ functions [81]:

$$S_{\rm TL}^{\rm EPA} = y^* \frac{1 - y + \frac{y^2}{2} + \frac{Q^2}{4E^2} - \frac{m_e^2}{Q^2}\left(y^2 + \frac{Q^2}{E^2}\right)}{y^2 + \frac{Q^2}{E^2}}, \quad (43)$$

$$S_{\rm L}^{\rm EPA} = \frac{y^*}{2}\left(1 - \frac{2m_e^2}{Q^2}\right), \quad (44)$$

where $y^* = \sqrt{y^2 + \frac{Q^2}{E^2}}$. As for the cross-sections, it was proposed in [81] to use $\sigma_{\rm L} = 0$ for all Q^2,

$$\sigma_{\rm T} = \nu\sigma_\gamma(\nu)Ey^* \quad (45)$$

for $Q^2 < m_\rho^2$, and $\sigma_{\rm T} = 0$ for $Q^2 > m_\rho^2$. But experimentally $R = \frac{\sigma_{\rm L}}{\sigma_{\rm T}}$ is approximately 0.33 at $Q^2 = m_\rho^2$ [82] and then slowly drops to about 0.2 at $Q^2 = 10\,{\rm GeV}^2$. The R1998 fit can be found in [83]. In addition, at large Q^2, the $\sigma_\gamma(\nu)$ cross-section must be substituted by the $\sigma_\gamma(K)$ value, where $K = \frac{W^2 - M^2}{2M} = \nu(1-x)$ is the momentum of the real photon corresponding to the same $W^2 = M^2 + 2MK = M^2 + 2M\nu - Q^2$ as for the virtual photon. For example, for Q^2 close to zero at $\nu \simeq 300\,{\rm MeV}$ the $\sigma_{\gamma^* p}$ cross-section reaches the maximum value (about 0.5 mb), and for virtual photons with $Q^2 = 0.28\,{\rm GeV}^2$ and $\nu = 300\,{\rm MeV}$ the cross-section is zero as it is below the pion production threshold.

In electronuclear physics another approach proposed by L. Hand [84] is popular. This approach is based on the transverse photon flux (TPF) definition. The longitudinal photon flux is considered only via the ϵ parameter, which is the ratio of the flux of longitudinal photons to that of transverse photons. The ϵ parameter is calculated as

$$\epsilon = 1 - \frac{2(\nu^2 + Q^2)}{(2E - \nu)^2 + \nu^2 + Q^2}, \quad (46)$$

where $\nu = E - E'$ is the photon energy. The differential cross-section of the electronuclear scattering can be written as

$$\frac{{\rm d}^2\sigma}{{\rm d}\Omega{\rm d}E'} = \Gamma_{\rm T} \cdot (\sigma_{\rm T} + \epsilon \cdot \sigma_{\rm L}), \quad (47)$$

$$\Gamma_{\rm T} = \frac{\alpha}{2\pi^2}\frac{K}{Q^2}\frac{E'}{E}\frac{1}{1-\epsilon}, \quad (48)$$

which gives in terms of eq. (42)

$$S_{\rm TL}^{\rm TPF} = y(1-x)\frac{1 - y + \frac{y^2}{2} + \frac{Q^2}{4E^2}}{y^2 + \frac{Q^2}{E^2}}, \quad (49)$$

$$S_{\rm L}^{\rm TPF} = \frac{y}{2}(1-x). \quad (50)$$

Comparison with eqs. (43),(44) shows that, even at $\frac{Q^2}{\nu^2} \to 0$ and $\frac{m_e^2}{Q^2} \to 0$, the Hand formula differs by the factor $(1-x)$ (where $x = \frac{Q^2}{2M\nu}$). Nevertheless, in the $Q^2 \to 0$ limit it coincides with the EPA calculations. The TPF approach has a natural normalization for the cross-section for interaction of the virtual photon with a nucleus. It is defined as

$$\sigma_{\gamma^*} = \sigma_{\rm T} + \epsilon \cdot \sigma_{\rm L}. \quad (51)$$

The third approach is developed for the analysis of deep-inelastic scattering (DIS) reactions. It is based on a consideration of the F_1 and F_2 structure functions calculated in the framework of the parton model. The DIS formula for the differential cross-section of the electronuclear interaction [5] is

$$\frac{{\rm d}^2\sigma}{{\rm d}x{\rm d}y} = \frac{4\pi\alpha^2}{Q^2}\left(\frac{1-y}{xy}F_2 + yF_1 - xy\frac{M^2}{Q^2}F_2\right). \quad (52)$$

For small Q^2, when the $\frac{m_e^2}{Q^2}$ factor must be taken into account, the differential cross-section is calculated in [85] as

$$\frac{y{\rm d}^2\sigma}{{\rm d}y{\rm d}Q^2} = \frac{4\pi\alpha^2}{Q^4}\left[\left(1 - y - \frac{Q^2}{4E^2}\right)F_2 + \left(1 - \frac{2m_e^2}{Q^2}\right)xy^2F_1\right], \quad (53)$$

where

$$F_1 = \frac{M\nu}{4\pi^2\alpha}\left(\sigma_{\rm T} + \frac{Q^2}{\nu^2}(\sigma_{\rm T} + \sigma_{\rm L})\right), \quad (54)$$

$$F_2 = \frac{Q^2}{4\pi^2\alpha}(\sigma_{\rm T} + \sigma_{\rm L}). \quad (55)$$

Substituting eqs. (54),(55) into eq. (53) it is easy to show that

$$S_{\rm TL}^{\rm DIS} = \frac{1 - y + \frac{y^2}{2} + \frac{Q^2}{4E^2} - \frac{m_e^2}{Q^2}\left(y^2 + \frac{Q^2}{E^2}\right)}{y}, \quad (56)$$

$$S_{\rm L}^{\rm DIS} = \frac{y}{2}\left(1 - \frac{2m_e^2}{Q^2}\right). \quad (57)$$

These terms coincide with eqs. (43),(44) in the $\frac{Q^2}{\nu^2} \to 0$ limit. It is important to point out that in DIS (based on the light cone approach) the y value is defined as $y^{\rm DIS} = 1 - \frac{E'}{E}\cos\theta = y + \frac{Q^2}{2E^2}$. The usual DIS assumption is $y^{\rm DIS} = y$, so all the terms proportional to $\frac{Q^2}{2E^2}$ must be considered to be negligible in the DIS formulas otherwise the definition of y is unclear. In this sense the final DIS formula for $m_e^2 \ll Q^2 \ll \nu^2$ can be simplified to

$$\frac{xy{\rm d}^2\sigma}{{\rm d}x{\rm d}y} = \frac{4\pi\alpha^2}{Q^2}\left((1-y)F_2 + y^2xF_1\right), \quad (58)$$

with $F_1 = \frac{M\nu}{4\pi\alpha^2}\sigma_{\rm T}$ and $F_2 = \frac{Q^2}{4\pi\alpha^2}(\sigma_{\rm T} + \sigma_{\rm L})$.

To take into account the mass of the electron at low Q^2 where the electronuclear cross-section is very large, the ϵ and the $\Gamma_{\rm T}$ parameters of the TPF approach must be redefined as

$$\epsilon = 1 - \frac{2(\nu^2 + Q^2)\left(1 - \frac{2m_e^2}{Q^2}\right)}{(2E - \nu)^2 + (\nu^2 + Q^2)\left(1 - \frac{4m_e^2}{Q^2}\right)}, \quad (59)$$

$$\Gamma_{\rm T} = \frac{\alpha}{2\pi^2}\frac{K}{Q^2}\frac{E'}{E}\frac{1-\frac{2m_e^2}{Q^2}}{1-\epsilon}. \quad (60)$$

This transforms the TPF eqs. (49),(50) to

$$S_{\rm TL}^{\rm TPF} = y(1-x)\frac{1-y+\frac{y^2}{2}+\frac{Q^2}{4E^2}-\frac{m_e^2}{Q^2}\left(y^2+\frac{Q^2}{E^2}\right)}{y^2+\frac{Q^2}{E^2}}, \quad (61)$$

$$S_{\rm L}^{\rm TPF} = \frac{y}{2}\left(1-\frac{2m_e^2}{Q^2}\right)(1-x). \quad (62)$$

For simplicity, in all calculations shown here the universal $S_{\rm TL}$ and $S_{\rm L}$ functions are used in the form

$$S_{\rm TL} = y\frac{1-y+\frac{y^2}{2}+\frac{Q^2}{4E^2}-\frac{m_e^2}{Q^2}\left(y^2+\frac{Q^2}{E^2}\right)}{y^2+\frac{Q^2}{E^2}}, \quad (63)$$

$$S_{\rm L} = \frac{y}{2}\left(1-\frac{2m_e^2}{Q^2}\right). \quad (64)$$

In fact, because of eq. (45) the authors of [81] end up with the same normalization of the cross-section. The normalization of the cross-section defined by eqs. (63),(64) coincides with the normalization by eqs. (56),(57) in the DIS $y \gg \frac{Q^2}{2E^2}$ limit. The normalization of the TPF cross-sections differs only by the $(1-x)$ factor which is used in the $\sigma_{\gamma^* p}$ approximation below. Using eq. (51) the differential cross-section of the electronuclear scattering can be written as

$$\frac{{\rm d}^2\sigma_{eA}}{{\rm d}y{\rm d}Q^2} = \frac{\alpha y}{\pi Q^2}\left(\frac{(1-\frac{y}{2})^2}{y^2+\frac{Q^2}{E^2}}+\frac{1}{4}-\frac{m_e^2}{Q^2}\right)\sigma_{\gamma^* A}, \quad (65)$$

where $\sigma_{\gamma^* A} = \sigma_{\gamma A}(\nu)$ for small Q^2 and must be approximated as a function of ϵ, ν, and Q^2 for large Q^2. Interactions of longitudinal photons are included in the effective $\sigma_{\gamma^* A}$ cross-section through the ϵ factor, defined by eq. (59).

6.2 Approximation of the Q^2-dependence of electronuclear reactions

The electronuclear problem, in the sense of interaction of virtual photons with nuclei, can thus be split into two. At small Q^2 it is possible to use the $\sigma_\gamma(\nu)$ cross-section. In the $Q^2 \gg m_e^2$ region it is necessary to calculate the effective $\sigma_{\gamma^*}(\epsilon,\nu,Q^2)$ cross-section.

Following the EPA notation the differential cross-section of electronuclear scattering can be connected with the number of equivalent photons ${\rm d}n = \frac{{\rm d}\sigma}{\sigma_{\gamma^*}}$. For $y \ll 1$ and $Q^2 < 4m_e^2$ the canonical method [86] leads to the simple result

$$\frac{y{\rm d}n(y)}{{\rm d}y} = -\frac{2\alpha}{\pi}\ln(y). \quad (66)$$

In [81] the integration over Q^2 for $\nu^2 \gg Q^2_{\rm max} \simeq m_e^2$ leads to

$$\frac{y{\rm d}n(y)}{{\rm d}y} = -\frac{\alpha}{\pi}\left(\frac{1+(1-y)^2}{2}\ln\left(\frac{y^2}{1-y}\right)+(1-y)\right). \quad (67)$$

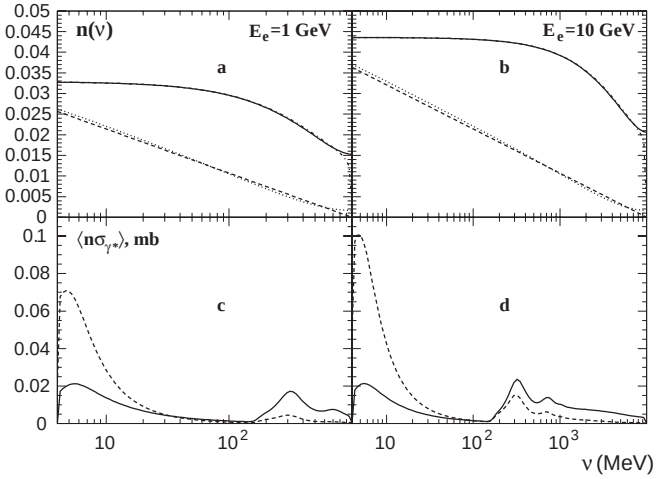

Fig. 12. Relative contribution of equivalent photons with small Q^2 to the total "photon flux" for 1 GeV electrons (a) and 10 GeV electrons (b). In figures (c) and (d) the equivalent photon distribution ${\rm d}n(\nu,Q^2)$ is multiplied by the photonuclear cross-section $\sigma_{\gamma^*}(K,Q^2)$ and integrated over Q^2 in two regions: the dashed lines are integrals over the low-Q^2 equivalent photons (under the dashed line in the first two figures), and the solid lines are integrals over the high-Q^2 equivalent photons (above the dashed lines in the first two figures).

In the $y \ll 1$ limit this formula converges to eq. (66). But the correspondence with eq. (66) can be made more explicit if the exact integral

$$\frac{y{\rm d}n(y)}{{\rm d}y} = \frac{\alpha}{\pi}\left(\frac{1+(1-y)^2}{2}l_1-(1-y)l_2-\frac{(2-y)^2}{4}l_3\right), \quad (68)$$

where $l_1 = \ln\left(\frac{Q^2_{\rm max}}{Q^2_{\rm min}}\right)$, $l_2 = 1-\frac{Q^2_{\rm min}}{Q^2_{\rm max}}$, $l_3 = \ln\left(\frac{y^2+Q^2_{\rm max}/E^2}{y^2+Q^2_{\rm min}/E^2}\right)$, $Q^2_{\rm min} = \frac{m_e^2y^2}{1-y}$, is calculated for

$$Q^2_{\rm max(}m_e{\rm)} = \frac{4m_e^2}{1-y}. \quad (69)$$

(the $(1-y)$ factor is arbitrary used to keep $Q^2_{\rm max(}m_e{\rm)} > Q^2_{\rm min}$), which can be considered as a boundary between the low and the high-Q^2 regions. The full transverse photon flux can be calculated as an integral of eq. (68) with the maximum possible upper limit

$$Q^2_{\rm max(max)} = 4E^2(1-y). \quad (70)$$

The full transverse photon flux can be approximated by

$$\frac{y{\rm d}n(y)}{{\rm d}y} = -\frac{2\alpha}{\pi}\left(\frac{(2-y)^2+y^2}{2}\ln(\gamma)-1\right), \quad (71)$$

where $\gamma = \frac{E}{m_e}$. It must be pointed out that neither this approximation nor eq. (68) work at $y \simeq 1$, as at this point $Q^2_{\rm max(max)}$ becomes smaller than $Q^2_{\rm min}$. The formal limit of the method is $y < 1-\frac{1}{2\gamma}$.

In fig. 12(a),(b) the energy distribution for the equivalent photons is shown. The low-Q^2 photon flux with the

upper limit defined by eq. (69)) is compared with the full photon flux. The low-Q^2 photon flux is calculated using eq. (66) (the dashed lines) and using eq. (68) (the dotted lines). The full photon flux is calculated using eq. (71) (the solid lines) and using eq. (68) with the upper limit defined by eq. (70) (the dash-dotted lines, which differ from the solid lines only at $\nu \approx E_e$). The conclusion is that to calculate either the number of low-Q^2 equivalent photons or the total number of equivalent photons one can use the simple approximations given by eq. (66) and eq. (71), respectively, instead of using eq. (68), which cannot be integrated over y analytically. Comparing the low-Q^2 photon flux and the total photon flux it is possible to show that the low-Q^2 photon flux is about half of the total. From the interaction point of view the decrease of σ_{γ^*} with increasing Q^2 must be taken into account. The cross-section reduction for the virtual photons with large Q^2 is governed by two factors. First, the cross-section drops with Q^2 as a squared dipole nucleonic form factor

$$G_D^2(Q^2) \approx \left(1 + \frac{Q^2}{(843\,\mathrm{MeV})^2}\right)^{-2}. \qquad (72)$$

Second, all the thresholds of the γA reactions are shifted to higher ν by a factor $\frac{Q^2}{2M}$, which is the difference between the K and ν values. Following the method proposed in [87] the σ_{γ^*} at large Q^2 can be approximated as

$$\sigma_{\gamma*} = (1-x)\sigma_\gamma(K)G_D^2(Q^2)e^{b(\epsilon,K)\cdot r + c(\epsilon,K)\cdot r^3}, \qquad (73)$$

where $r = \frac{1}{2}\ln(\frac{Q^2+\nu^2}{K^2})$. The ϵ-dependence of the $a(\epsilon, K)$ and $b(\epsilon, K)$ functions is weak, so for simplicity the $b(K)$ and $c(K)$ functions are averaged over ϵ. They can be approximated as

$$b(K) \approx \left(\frac{K}{185\,\mathrm{MeV}}\right)^{0.85}, \qquad (74)$$

$$c(K) \approx -\left(\frac{K}{1390\,\mathrm{MeV}}\right)^{3}. \qquad (75)$$

As the [87] approximation is made in the TPF normalization, it must be corrected by a $(1-x)$ factor. At large Q^2 the nuclear shadowing function $s_p(A)$ expressed in eq. (27), which was used for the approximations of the photonuclear cross-section, can converge to 1 with increasing Q^2 as the shadowing effect seems to be smaller for virtual photons [88], but at present this effect is not well measured. The low energy nature of the GDR effects proves that the additional form factor must be used for σ_{γ^*} in the GDR region, but this effect is also unmeasured. Neither effect is implemented in the GEANT4 simulation of electronuclear reactions.

An alternative method for approximating σ_{γ^*}, which uses the nuclear structure functions for the cross-section approximation, can be found in [89], but at small K this method is inappropriate as it is correct only in the sense of the Bloom-Gilman duality [90], in that it describes only the mean cross-section instead of the resonance shape of the cross-section. It is appropriate only for $K > 1260\,\mathrm{MeV}$. Other methods for approximating σ_{γ^*} can be found in [85].

The result of the integration of the photon flux multiplied by the cross-section approximated by eq. (73) is shown in fig. 12(c,d). The integrated cross-sections are shown separately for the low-Q^2 region ($Q^2 < Q^2_{\max(m_e)}$, dashed lines) and for the high-Q^2 region ($Q^2 > Q^2_{\max(m_e)}$, solid lines). These functions must be integrated over $\ln(\nu)$, so it is clear that because of the GDR contribution the low-Q^2 part covers more than half of the total $eA \to hadrons$ cross-section. But at $\nu > 200\,\mathrm{MeV}$, where the multiplicity of hadrons increases, the large Q^2 part dominates. In this sense, for the better simulation of the hadronic production by electrons it is necessary to simulate the high-Q^2 part as well as the low-Q^2 part.

6.3 Randomization of electronuclear reactions

The low-Q^2 equivalent photons have already been implemented in GEANT4 on the basis of eq. (66). The electronuclear cross-section is calculated as

$$\frac{\pi\sigma_{eA}}{2\alpha} = \ln(E_e)\cdot I_1(E_e) - I_2(E_e), \qquad (76)$$

$$I_1(E) = \int^E \sigma_{\gamma A}(\nu)\mathrm{d}\ln(\nu), \qquad (77)$$

$$I_2(E) = \int^E \ln(\nu)\sigma_{\gamma A}(\nu)\mathrm{d}\ln(\nu), \qquad (78)$$

where the integration is done from the threshold of the γA reaction (E_e is the electron energy). The integral functions $I_1(x)$ and $I_2(x)$ are calculated for 14 nuclei and the A-dependence is interpolated. Using these integral functions the particular eA interaction cross-section is calculated for the fixed E_e of the incident electron. After the cross-section has been calculated, the value of $\ln(E_e)\cdot I_1(E_e) - I_2(E_e)$ is known and can be used for the randomization of the equivalent photon energy ν, which can be obtained from the equation

$$\ln(\nu)\cdot I_1(\nu) - I_2(\nu) = R\cdot(\ln(E_e)\cdot I_1(E_e) - I_2(E_e)), \qquad (79)$$

where R is a random number ($0 < R < 1$).

Using the same approach, but taking into account the contribution of high-Q^2 photons it is possible to use eq. (71) with the overestimated $\sigma_{\gamma^*A} = \sigma_{\gamma A}(\nu)$ cross-section. Then the slightly overestimated electronuclear cross-section is calculated as

$$\sigma^*_{eA} = (2\ln(\gamma) - 1)\cdot J_1 - \frac{\ln(\gamma)}{E_e}\left(2J_2 - \frac{J_3}{E_e}\right), \qquad (80)$$

where

$$J_1(E_e) = \frac{\alpha}{\pi}\int^{E_e} \sigma_{\gamma A}(\nu)\mathrm{d}\ln(\nu), \qquad (81)$$

$$J_2(E_e) = \frac{\alpha}{\pi}\int^{E_e} \nu\sigma_{\gamma A}(\nu)\mathrm{d}\ln(\nu), \qquad (82)$$

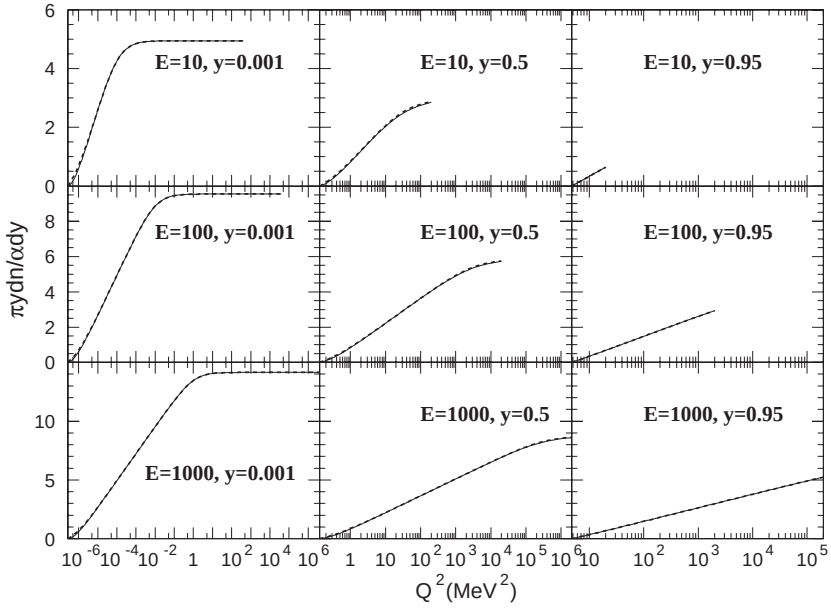

Fig. 13. Integrals of Q^2 spectra of virtual photons for three energies 10 MeV, 100 MeV, and 1 GeV at $y = 0.001$, $y = 0.5$, and $y = 0.95$. The solid line corresponds to eq. (68) and the dashed line (which almost everywhere coincides with the solid line) corresponds to eq. (68).

$$J_3(E_e) = \frac{\alpha}{\pi}\int^{E_e} \nu^2 \sigma_{\gamma A}(\nu) \mathrm{d}\ln(\nu). \quad (83)$$

Similarly to eq. (79), the equivalent photon energy $\nu = yE$ can be obtained for the particular random number R from the equation

$$R = \frac{(2\ln(\gamma)-1)J_1(\nu) - \frac{\ln(\gamma)}{E_e}\left(2J_2(\nu) - \frac{J_3(\nu)}{E_e}\right)}{(2\ln(\gamma)-1)J_1(E_e) - \frac{\ln(\gamma)}{E_e}\left(2J_2(E_e) - \frac{J_3(E_e)}{E_e}\right)}. \quad (84)$$

Equation (68) is too complicated for the randomization of Q^2 but there is an easily randomized formula which approximates eq. (68) above the hadronic threshold ($E > 10$ MeV)

$$\frac{\pi}{\alpha D(y)}\int_{Q^2_{\min}}^{Q^2} \frac{y\mathrm{d}n(y,Q^2)}{\mathrm{d}y\mathrm{d}Q^2}\mathrm{d}Q^2 = -L(y,Q^2) - U(y), \quad (85)$$

where

$$D(y) = 1 - y + \frac{y^2}{2}, \quad (86)$$

$$L(y,Q^2) = \ln\left(F(y) + \left(e^{P(y)} - 1 + \frac{Q^2}{Q^2_{\min}}\right)^{-1}\right), \quad (87)$$

$$F(y) = \frac{(2-y)(2-2y)}{y^2}\cdot\frac{Q^2_{\min}}{Q^2_{\max}}, \quad (88)$$

$$U(y) = P(y)\cdot\left(1 - \frac{Q^2_{\min}}{Q^2_{\max}}\right), \quad (89)$$

$$P(y) = \frac{1-y}{D(y)}. \quad (90)$$

The Q^2 value can then be calculated as

$$\frac{Q^2}{Q^2_{\min}} = 1 - e^{P(y)} + \left(e^{R\cdot L(y,Q^2_{\max}) - (1-R)\cdot U(y)} - F(y)\right)^{-1}, \quad (91)$$

where R is a random number. In fig. 13, eq. (68) (the solid curve) is compared to eq. (85) (the dashed curve). As the two curves are almost indistinguishable in the figure, it can be used for the illustration of the Q^2 spectrum of virtual photons, which is a derivative of these curves. An alternative approach is to use eq. (68) for the randomization with a three-dimensional table $\frac{y\mathrm{d}n}{\mathrm{d}y}(Q^2, y, E_e)$.

After the ν and Q^2 values have been found, the value of $\sigma_{\gamma^* A}(\nu, Q^2)$ is calculated using eq. (73). If $R\cdot\sigma_{\gamma A}(\nu) > \sigma_{\gamma^* A}(\nu, Q^2)$, no interaction occurs and the electron keeps going. This "do nothing" process has low probability and cannot shadow other processes.

7 Conclusion

The photonuclear cross-sections are approximated for any energy and for any nucleus but there can still be individual effects for particular nuclei. It is very interesting to measure the photonuclear cross-sections in the GDR region for ^{3}He, ^{10}B, and ^{11}B nuclei, which are expected to be anomalous. Measurements for the same nuclei together with measurements for ^{6}Li in the resonance region and at high energies can clarify how the high resonances "melt" in nuclei with increasing A.

The new approach to the GDR approximation must be tested experimentally and interpreted theoretically. If the A-dependent g_i contributions are understood theoretically or in the framework of some model, it can help to

calculate the residual nucleus excitation in the "knock-out" electronuclear reactions. This is very important for the simulation of electronuclear reactions.

Electronuclear reactions are not exhaustively covered in this paper. But the reminder (elastic and quasielastic reactions on nuclei) is not connected with photonuclear cross-sections. Some basic ideas concerning this issue can be found in Stein's paper [84]. The most up-to-date analysis for the quasielastic reactions is beyond the scope of this paper, but it is very important to include these reactions in the simulation because, as was demonstrated in [4], the quasielastic "knock out" reactions can be successfully simulated by the CHIPS model.

The solution found for the simulation of the high-Q^2 part of electronuclear reactions is good enough for the GEANT4 simulation, which must be fast and easily randomized. But the simulation method must be compared with at least one point of the $\sigma_{eA\to\text{hadrons}}$ cross-section, which unfortunately has not been found in published papers. Only empirical integrations of the differential cross-sections of (e,p) [91] and (e,π^+) [92] reactions exist.

Another possible application of this method is in muon-nuclear reactions. At present muon-nuclear reactions are implemented in GEANT4 for high energies ($E_\mu > 10\,\text{GeV}$) and large ν ($y > 0.01$, $\nu > m_\pi$). Simulation of muon-nuclear reactions for relatively large Q^2 is necessary, as muons are deeply penetrating particles and the scattering of muons, even at relatively small angles, is very important. The method developed in this paper can be used to improve this simulation.

It is a pleasure to thank Prof. H. Hirayama, Dr. P. Degtyarenko, Dr. J.-P. Wellisch and Dr. M. Sang for useful discussions. This work was partially supported by the grant CERN-INTAS 99-0377.

References

1. S. Giani *et al.*, GEANT4: Object Oriented Toolkit for Simulation in HEP, LCB status report CERN/LHCC/98-44, November 1998.
2. P.V. Degtyarenko, M.V. Kossov, H.P. Wellisch, Eur. Phys. J. A **8**, 217 (2000).
3. P.V. Degtyarenko, M.V. Kossov, H.P. Wellisch, Eur. Phys. J. A **9**, 411 (2001).
4. P.V. Degtyarenko, M.V. Kossov, H.P. Wellisch, Eur. Phys. J. A **9**, 421 (2001).
5. Particle Data Group, *Review of Particle Physics*, Eur. Phys. J. C **15**, 238 (2000).
6. M. MacCormick *et al.*, Phys. Rev. C **53**, 41 (1996).
7. The ZEUS Collaboration, Eur. Phys. J. C **7**, 609 (1999).
8. R.A. Arndt *et al.*, Phys. Rev. C **53**, 430 (1996).
9. O. Klein, Y. Nishina, Z. Phys. **52**, 853 (1929).
10. J.L. Powell, Phys. Rev. **75**, 32 (1949).
11. V.A. Petrun'kin, Sov. Phys. JETP **13**, 808 (1961); Sov. J. Part. Nucl. **12**, 278 (1981).
12. V. Olmos de Leon *et al.*, Eur. Phys. J. A **10**, 207 (2001).
13. J.R. Cudell *et al.*, Phys. Rev. D **61**, 034019 (2000).
14. M. Froissart, Phys. Rev. **123**, 1053 (1961).
15. M.M. Block, R.N. Cahn, Rev. Mod. Phys. **57**, 563 (1985).
16. J. Ahrens *et al.*, Nucl. Phys. A **251**, 479 (1975).
17. J. Ahrens *et al.*, in *Photopion Nuclear Physics*, edited by P. Stoler (Plenum, New York, 1979) p. 385.
18. A.S. Aleksanian *et al.*, Sov. J. Nucl. Phys. **45**, 628 (1987).
19. E.A. Arakelian *et al.*, Phys. Lett. B **79**, 143 (1978).
20. E.A. Arakelian *et al.*, Sov. J. Nucl. Phys. **38**, 589 (1983).
21. E.A. Arakelian *et al.*, Sov. J. Nucl. Phys. **42**, 1 (1985).
22. E.A. Arakelian *et al.*, Sov. J. Nucl. Phys. **52**, 878 (1990).
23. J. Arends *et al.*, Phys. Lett. B **98**, 423 (1981).
24. Yu. M. Arkatov *et al.*, Yad.. Fiz. **31**, 1400 (1980).
25. T.A. Armstrong *et al.*, Nucl. Phys. B **41**, 445 (1972).
26. Y.I. Assafiri, M.N. Thompson, Nucl. Phys. A **460**, 455 (1986).
27. A.D. Bates *et al.*, Phys. Rev. C **40**, 506 (1989).
28. N. Bezic *et al.*, Nucl. Phys. A **128**, 426 (1969).
29. N. Bianchi *et al.*, Phys. Lett. B **299**, 219 (1993).
30. N. Bianchi *et al.*, Phys. Lett. B **325**, 333 (1994).
31. N. Bianchi *et al.*, Phys. Rev. C **54**, 1688 (1996).
32. O.V. Bogdankevich *et al.*, Sov. Phys. JETP **42**, 1044 (1962).
33. G.R. Brookes *et al.*, Phys. Rev. D **8**, 2826 (1973).
34. N.A. Burgov *et al.*, Zh. Eksp. Teor. Fiz. **45**, 1694 (1963).
35. D.O. Caldwell *et al.*, Phys. Rev. D **7**, 1362 (1973).
36. C. Chollet *et al.*, Phys. Lett. B **127**, 331 (1983).
37. D.O. Caldwell *et al.*, Phys. Rev. Lett. **42**, 553 (1979).
38. B.S. Dolbilkin *et al.*, Izv. AN SSSR, **2**, 349 (1966).
39. B.S. Dolbilkin *et al.*, Sov. J. Nucl. Phys. **9**, 534 (1969).
40. B.S. Dolbilkin *et al.*, Pisma Zh. Eksp. Teor. Fiz. **10**, 365 (1969).
41. J. Dular *et al.*, Nucl. Phys. **14**, 131 (1959/60).
42. D. Ehhalt, R. Kosiek, R. Pfeiffer, Z. Phys. **154**, 569 (1959).
43. Th. Frommhold *et al.*, Phys. Lett. B **295**, 28 (1992).
44. S.C. Fultz *et al.*, Phys. Rev. **186**, 1255 (1969).
45. B.I. Gavrilov, L.E. Lazareva, Sov. Phys. JETP **3**, 871 (1957).
46. M.L. Ghedira, in *Proceedings of the 8ème Session de Physique Nuclèaire* (Aussois, 1985), S. 9-1.
47. G.M. Gurevich *et al.*, Pisma Zh. Eksp. Teor. Fiz. **20**, 741 (1974).
48. G.M. Gurevich *et al.*, Nucl. Phys. A **273**, 326 (1976).
49. G.M. Gurevich *et al.*, Pisma. Zh. Eksp. Teor. Fiz. **23**, 411 (1976).
50. G.M. Gurevich *et al.*, Probl. Yad. Fiz. **8**, 106 (1978).
51. G.M. Gurevich *et al.*, Nucl. Phys. A **351**, 257 (1981).
52. V. Heynen *et al.*, Phys. Lett. B **34**, 651 (1971).
53. B.S. Ishkhanov *et al.*, Sov. J. Nucl. Phys. **33**, 303 (1981).
54. A. Lepretre *et al.*, Nucl. Phys. A **367**, 237 (1981).
55. P. Levi Sandri *et al.*, Phys. Rev. C **39**, 1701 (1989).
56. M. MacCormick *et al.*, Phys. Rev. C **55**, 1033 (1997).
57. S. Michalowski *et al.*, Phys. Rev. Lett. **39**, 737 (1977).
58. U. Miklavzic *et al.*, Nucl. Phys. **31**, 570 (1962).
59. V. Muccifora *et al.*, Phys. Rev. C **60**, 64616 (1999).
60. J.W. Norbury *et al.*, Austr. J. Phys. **31**, 471 (1978).
61. F. Partovi *et al.*, Ann. Phys. (N.Y.) **27**, 79 (1964).
62. R.A. Sutton *et al.*, Nucl. Phys. A **398**, 257 (1983).
63. Yu. I. Sorokin, B.A. Yur'ev, Sov. J. Nucl. Phys. **20**, 123 (1975).
64. Yu. I. Sorokin, B.A. Yur'ev, Izv. AN SSSR, **39**, 114 (1975).
65. V.V. Varlamov *et al.*, CDFE/Li2,86, taken from the EXFOR database.
66. A. Veyssiere *et al.*, Nucl. Phys. A **159**, 561 (1970).
67. V.G. Vlasenko *et al.*, Sov. J. Nucl. Phys. **23**, 265 (1976).
68. J.M. Wyckoff *et al.*, Phys. Rev. **137**, B576 (1965).

69. B. Ziegler, Lect. Notes Phys. Vol. **108** (Springer, Berlin, 1979) p. 148.
70. S. Brodsky, F. Close, J. Gunion, Phys. Rev. D **6**, 177 (1972).
71. P. Carlos *et al.*, Nucl. Phys. A **431**, 573 (1984).
72. A.S. Penfold, J.E. Leiss, Phys. Rev. **114**, 1332 (1959).
73. The Jefferson Lab Hall A Collaboration, Phys. Rev. Lett. **86**, 5670 (2001).
74. LAND Collaboration, Phys. Rev. Lett. **70**, 1767 (1993).
75. E. Fermi, Z. Phys. **29**, 315 (1924).
76. K.F. von Weizsacker, Z. Phys. **88**, 612 (1934), E.J. Williams, Phys. Rev. **45**, 729 (1934).
77. L.D. Landau, E.M. Lifshitz, Soc. Phys. **6**, 244 (1934).
78. I. Ya. Pomeranchuk, I.M. Shmushkevich, Nucl. Phys. **23**, 1295 (1961).
79. V.N. Gribov *et al.*, Zh. Eksp. Teor. Fiz. **41**, 1834 (1961).
80. S.J. Brodsky *et al.*, Phys. Rev. D **4**, 1532 (1971).
81. V.M. Budnev *et al.*, Phys. Rep. **15**, 181 (1975).
82. L.H. Tao *et al.*, Z. Phys. C **70**, 387 (1996).
83. K. Abe *et al.*, Phys. Lett. B **452**, 194 (1999).
84. L.N. Hand, Phys. Rev. **129**, 1834 (1963); see also S. Stein, Phys. Rev. D **12**, 1884 (1975).
85. B. Badelek, J. Kwiecinski, Warsaw University preprint IFD/1/1994 (1994).
86. L.D. Landau, E.M. Lifshitz, *Course of Theoretical Physics* Vol. **4**, part 1, *Relativistic Quantum Theory* (Pergamon Press) p. 351, The method of equivalent photons.
87. F.W. Brasse *et al.*, Nucl. Phys. B **110**, 413 (1976).
88. J. Eickmeyer *et al.*, Phys. Rev. Lett. **36**, 289 (1976).
89. F.W. Brasse *et al.*, Nucl. Phys. B **39**, 421 (1972).
90. E.D. Bloom, F.J. Gilman, Phys. Rev. Lett. **25**, 1140 (1970).
91. R.W. Lourie, L.B. Weinstein, Phys. Rev. C **42**, 441 (1990).
92. K. Shoda *et al.*, Nucl. Phys. A **486**, 512 (1988).